JOURNAL OF GEOPHYSICAL RESEARCH, VOL. 102, NO. D5, PAGES 6035-6045, MARCH 20, 1997

Aerosol size distribution models based on in situ measurements

John N. Porter and Antony D. Clarke

School of Ocean and Earth Science and Technology, University of Hawaii, Honolulu

Abstract. We present an aerosol size distribution model summarizing measurements of sulfate, sea salt, and dust aerosol obtained in the marine boundary layer and marine free troposphere. Stratospheric aerosol cases are not included here. Aerosols were sampled in both both clean background conditions and aged anthropogenic aerosol (>3 days) which had advected over the ocean. Model size distributions are developed for the sulfate accumulation mode, sea-salt coarse mode, and dust coarse mode. The data demonstrate that both the accumulation and coarse mode aerosol gradually shift to larger diameters as the aerosol mass increases. Based on this relationship, it is possible to estimate the size distribution based on aerosol mass. Comparisons with other aerosol models show significant differences, which suggest further measuring and modeling efforts are needed.

1. Introduction

Models of aerosol size distributions are employed for various research endeavors including optical climate studies, satellite algorithm development, visibility studies, cloud physics models, air pollution studies, and lidar studies. Frequently, this aerosol information remains poorly quantified, and much of what does exist consists of aerosol chemical mass measurements obtained from filters. These filter measurements provide aerosol composition but often not as a function of diameter. In order to convert these aerosol mass measurements to size distributions, a model of the aerosol size distribution as a function of aerosol mass is needed.

In the past, various aerosol models have been developed to describe the aerosol size distribution. *Shettle and Fenn* [1979] developed standard aerosol size distributions for rural, urban, and maritime aerosol and studied their optical properties as a function of relative humidity. *Woodcock* [1953] developed a model of the coarse mode sea salt (above ~0.9 μm diameter) based on salt impaction on glass slides. *Garthman* [1982, 1984] compiled aerosol measurements from various investigators [e.g., *Hoppel*, 1979] and developed a model to describe the size distribution of marine aerosol as a function of wind fetch and distance from land. The *World Climate Programme* [1983] report WCP-55 compiled aerosol information from various sources in order to develop "standard aerosol cases" to be used in clear sky calculations. More recently, *d'Almeida et al.* [1991] have compiled various studies and developed a global climatology of aerosol optical properties for Arctic, Antarctic, desert, continental, urban, and maritime regions. Based on these aerosol distributions, they have modeled aerosol optical properties on a global scale. In this paper we describe a new aerosol model based on in situ aerosol measurements. Comparisons are made with other models.

2. Regions Measured and Instrumentation

The aerosol measurements described here took place in various experiments which are shown in Figure 1. These include three ship experiments: (1) the 1987 Second Soviet American Gas and Aerosol Experiment (SAGA 2) across the Pacific and Indian Oceans, (2) the 1989 Third Soviet American Gas and Aerosol Experiment (SAGA 3) in the central Pacific, and (3) a 1991 trip of opportunity aboard the Japanese Research vessel *Kaiyoumaru* also in the central Pacific. Aerosol measurements were also performed on two aircraft experiments and include (1) the 1989 Central Pacific Atmospheric Chemistry Experiment (CPACE) and the 1992 Atlantic Stratus Transition Experiment (ASTEX). In addition, free troposphere aerosol measurements were taken at Mauna Loa Observatory during January-March 1988 (MABIE) [*Clarke and Porter*, 1991].

During these experiments, aerosol size distributions were measured with either/both a custom optical particle counter (OPC) and/or a differential mobility analyzer (DMA) (sometimes called an electrostatic aerosol classifier). The customized OPC sized particles from 0.16 up to 7.5 μm. Calibrations for the OPC were performed using latex spheres of various sizes and ammonium sulfate aerosol generated by the DMA [*Clarke*, 1991]. The DMA (TSI model 3071) was used in conjunction with a condensation nuclei counter (TSI model 3760) to measure the aerosol size distribution from 0.02 to 0.5 μm diameter following *Covert et al.* [1992]. For both systems, thermal volatility of the aerosol size distributions was used to infer the aerosol composition as being either sulfuric acid (volatile at 150° C), ammonium sulfate/bisulfate (volatile at 300° C) or sea salt, soot, or dust, which are not volatile at 300° C [*Clarke*, 1991]. During aircraft experiments, aerosols were sampled under isokinetic conditions to minimize large particle loss. System losses were calculated and applied [*Porter et al.*, 1992].

When atmospheric aerosols size distributions are plotted as volume distributions (as in Figure 2), two modes become evident. Below about 0.6 μm diameter, the accumulation mode is maintained by the coagulation of smaller particles and aqueous-phase oxidation of presursor gases as well as removed by rain [*Hoppel et al.*, 1994; *Pruppacher and Klett*, 1980]. The coarse mode (above 0.6-1 μm diameter) consists primarily of either salt spray or dust and is maintained by mechanical lifting by the wind. The two modes appear clearly in the examples shown in Figure 2, including the Hawaii volcano plume, several clean marine cases, and an aged dust case measured near Hawaii above the trade wind inversion.

Paper number 96JD03403.
0148-0227/97/96JD-03403$09.00

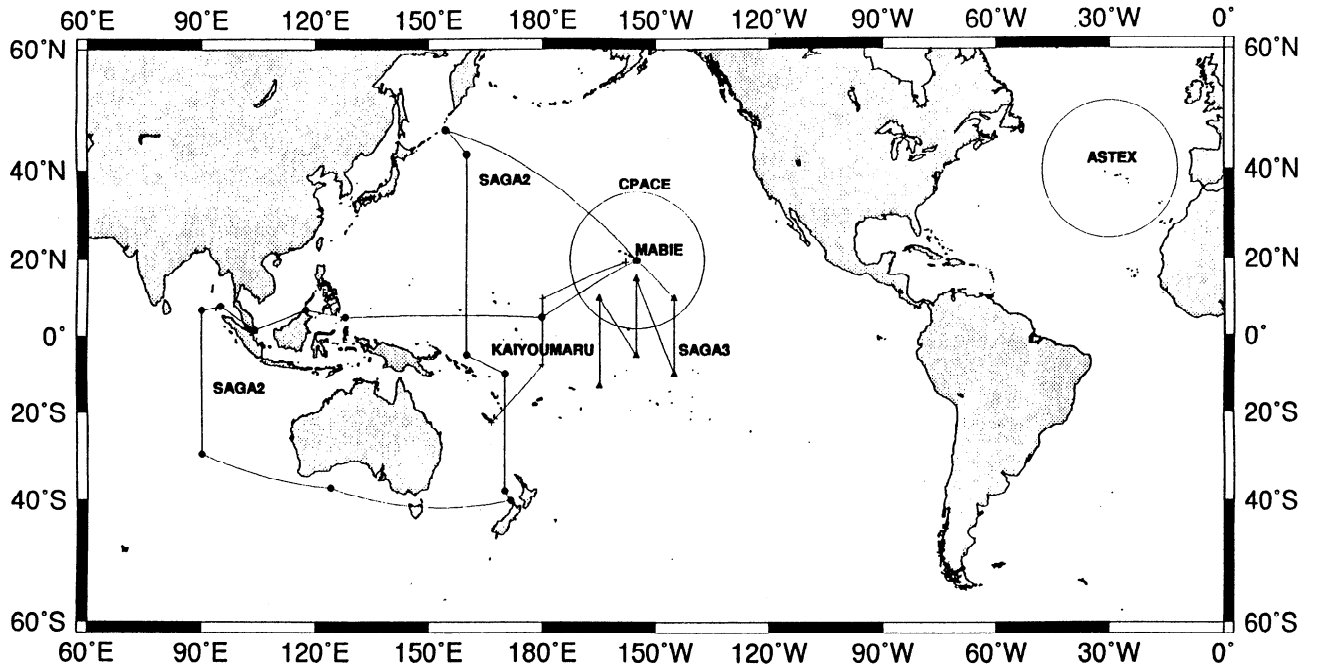

Figure 1. Map showing the location of various aerosol measurement experiments. Ship experiments are shown as lines. Aircraft experiments are shown as circles.

3. Accumulation Mode Size Distribution

In order to evaluate characteristics of the accumulation mode, DMA measurements (*Kaiyoumaru*, SAGA 3, and ASTEX) were used, as they provide information down to smaller sizes than the OPC and do not suffer from possible uncertainty in index of refraction. The first step in analyzing the collected DMA aerosol size distributions was to convert the measured distribution into a dry distribution by shifting each diameter downward. This operation was dependant on the measured relative humidities in the DMA (typically less than 15%) and the assumed aerosol compositions. The diameter shift was different for each distribution, but the average was near 13%. In carrying out this step, it was assumed that the common marine aerosol accumulation mode consists primarily of a mixture of sulfuric acid and ammonium bisulfate (i.e., a molar ratio of NH_4/SO_4 slightly less than 1). This composition and molar ratio assumption were based on aerosol volatility and ion chromatography (IC) measurements performed during the various experiments shown in Figure 1 [*Clarke*, 1991; *Clarke and Porter*, 1993]. In light of this frequently observed molar ratio fraction, laboratory studies were performed (using the combined OPC and DMA systems) with various NH_4/SO_4 molar ratio solutions from 0 to 1. The average of these results is shown in Figure 3 and is labeled "mixture." In the same figure the equilibrium drop sizes for sulfuric acid, ammonium bisulfate, and NaCl are shown [*Tang et al.*, 1977; *Tang and Munkelwitz*, 1977; *Tang*, 1980]. As might be expected, the laboratory results fall between the Tang et al. curves for sulfuric acid and ammonium bisulfate. For this paper, our laboratory results were used to convert the measured accumulation mode aerosol to dry diameters. The use of these same laboratory results has produced reasonable agreement when comparing OPC size distributions with filter ion chromatography (IC) measurements in the past [*Porter et al.*, 1992] and in comparing aerosol optical depth measurements with those calculated from size distributions [*Clarke et al.*, 1996].

The DMA size distributions were sorted and put into nine discrete categories based on dry aerosol volume. The dry distributions within each category were then averaged. In this way, all the low-volume cases were averaged together to obtain one size distribution and similarly for other aerosol volume ranges. For the present study, nine aerosol volume ranges were used: <0.05, 0.05-0.1, 0.1-0.2, 0.2-0.4, 0.4-0.8, 0.8-1.6, 1.6-3.2, 3.2-6.4, and 6.4-12.8 $\mu m^3/cm^3$. Assuming the accumulation mode dry aerosol density is the average of sulfuric acid and ammonium bisulfate, the aerosol density is then 1.81 and the corresponding aerosol mass categories employed here are <0.09, 0.09-0.2, 0.2-0.36, 0.36-0.72, 0.72-1.45, 1.45-2.9, 2.9-5.8, 5.8-11.6, 11.6-23.2 $\mu g/m^3$.

Figure 4a shows number distributions from SAGA 3 after sorting and averaging the measurements. Two predominant peaks appear: the Aitken mode at smaller sizes and the accumulation mode at larger sizes [*Covert et al.*, 1992]. Figure 4a, as well as the averages from the other experiments (not shown), indicate that the position of the Aitken mode is quite variable and can range from 0.02 to 0.09 μm diameter. The accumulation mode appears more well behaved and ranges between 0.1 and 0.3 μm diameter.

While the position of the Aitken mode is important for determining the number of aerosols which will become activated in clouds, for optical studies, we are interested in the aerosol scattering coefficient, which depends on the aerosol area distribution. In Figure 4b the averages from Figure 4a are plotted as area distributions. The Aitken mode contributes little to the total area and therefore is a small component of the aerosol optical properties. Figures 4c and 4d show the area distributions for the *Kaiyoumaru* and ASTEX experiments. Although the majority of the ASTEX size distributions were included in Figure 4d, some cases had a broader accumulation mode distribution. These cases are not shown here but were included in the modeling discussed below.

Figures 4b-4d show that the area distributions tend to shift to larger sizes as their concentration increases. This is further illus-

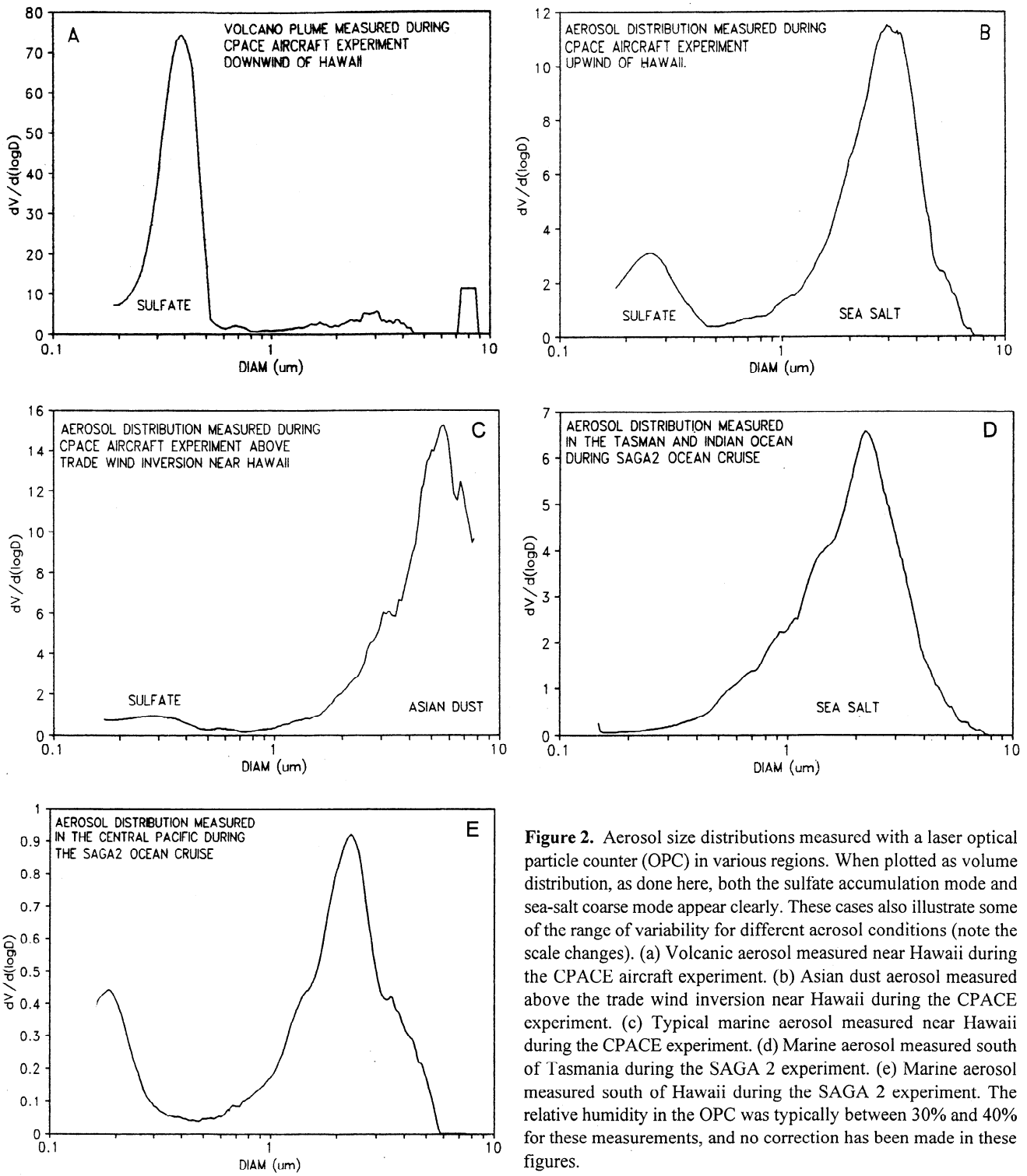

Figure 2. Aerosol size distributions measured with a laser optical particle counter (OPC) in various regions. When plotted as volume distribution, as done here, both the sulfate accumulation mode and sea-salt coarse mode appear clearly. These cases also illustrate some of the range of variability for different aerosol conditions (note the scale changes). (a) Volcanic aerosol measured near Hawaii during the CPACE aircraft experiment. (b) Asian dust aerosol measured above the trade wind inversion near Hawaii during the CPACE experiment. (c) Typical marine aerosol measured near Hawaii during the CPACE experiment. (d) Marine aerosol measured south of Tasmania during the SAGA 2 experiment. (e) Marine aerosol measured south of Hawaii during the SAGA 2 experiment. The relative humidity in the OPC was typically between 30% and 40% for these measurements, and no correction has been made in these figures.

trated in Figure 5, which shows the peak diameter of the area distributions for the SAGA 3, *Kaiyoumaru*, ASTEX and CPACE experiments. Each point corresponds to measurements ranging in duration from 15 min to 6 hours. Although there is significant variability, the trend to larger sizes as the aerosol dry mass increases is evident. Standard deviations, in the peak diameter, for the nine different mass ranges were 0.028, 0.023, 0.021, 0.015, 0.031, 0.035, 0.037, 0.023, 0.021 with an average of 0.027. For reference purposes, a line has been fit through the approximate center of the cases, and two outer lines are drawn at ±0.035, which is near the maximum range of standard deviation values.

Although it is well known that stratospheric aerosol can coagulate to large sizes, it has generally not been assumed that boundary aerosol might have a relationship between the aerosol mass and the peak diameter of the accumulation mode. This topic was studied by *Whitby* [1978] who found only a weak relationship between the two. Comparing his Figure 12, we see that his measurements fall in the top right of our Figure 5, as his measurements

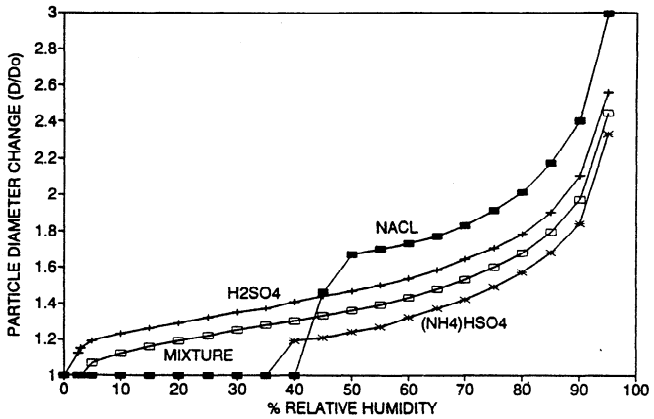

Figure 3. Equilibrium aerosol diameters as a function of relative humidity for various aerosol compositions. The values for NaCl, H_2SO_4 and $(NH_4)HSO_4$ are based on the work of *Tang et al.* [1977; *Tang and Munkelwitz*, 1977; *Tang*, 1980]. The line shown for the mixture is based on our laboratory experiments with various molar ratios of (NH_4/SO_4) ranging from 0 to 1.

represent larger aerosol concentrations. Therefore his measurements are not necessarily in conflict with our results. Unfortunately, it was not clear if he attempted to correct for different relative humidities in his instrument, so that exact comparisons are difficult. More recently, *Remer et al.* [1996] have derived the effective column aerosol size distribution from optical measurements of the Sun and the aureole. Similar to our results, they find a relationship between the accumulation mode mass and its effective size. Their measurements include a range of clean and polluted cases off the east coast of the United States.

In order to develop an overall size distribution model of the accumulation mode, similar DMA area average distributions from different experiments were grouped together (Figure 6). Next, an aerosol distribution model was created as the sum of two lognormal curves and was fit to the area distribution measurements. The use of two lognormal curves allowed better fitting of the narrow top and broad tail at the smaller sizes and therefore was used for all types of aerosol models developed in this paper. The use of a single lognormal curve was attempted, but we were not satisfied with the results. The lognormal equation used here follows *Reist* [1984] and is given by

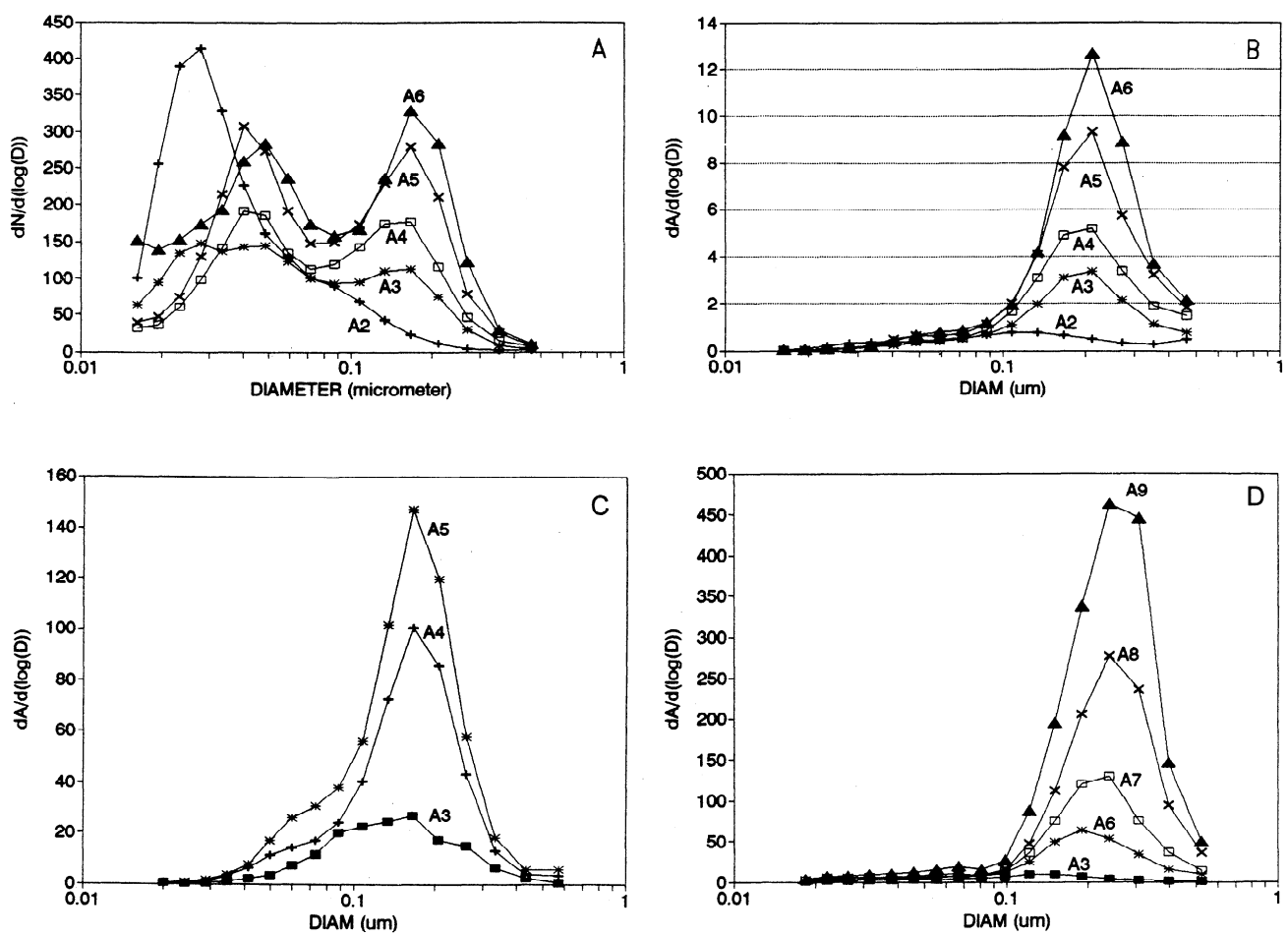

Figure 4. Average dry aerosol size distributions measured with the differential mobility analyzer during (a) SAGA 3 (number distribution), (b) SAGA 3 (area distribution), (c) *Kaiyoumaru* (area distribution), and (d) ASTEX (area distributions). Each distribution shown here is the average of many distributions which fell in a particular mass range. The SAGA 3 measurements (number distribution and area distribution) show that the smaller mode Aitken aerosols contribute little to the aerosol area distribution which is of optical interest.

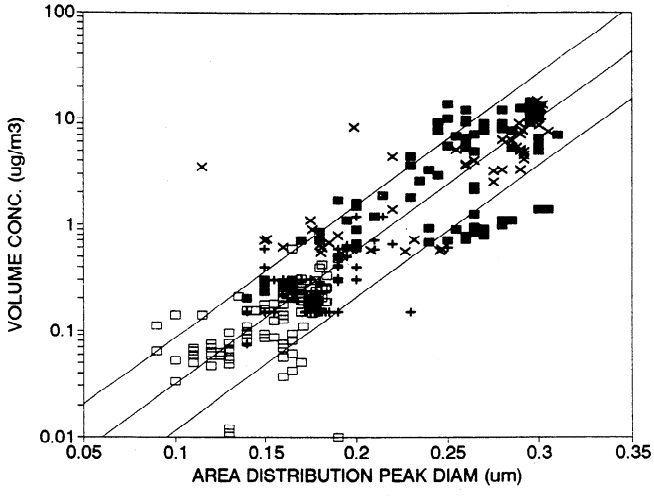

Figure 5. Peak diameter of the dry DMA size distribution plotted versus the aerosol dry volume. As the aerosol concentration increases, the aerosol distribution tends to move to larger sizes. Reference lines drawn at ±0.035 from the center are also drawn. Solid boxes correspond to ASTEX DMA measurements, open boxes are ship DMA measurements, and crosses are CPACE OPC measurements.

$$dN/dlogD = Curve1 + Curve2 \quad (1)$$

$$CurveX = \frac{N}{D \ln\sigma_g\sqrt{2\pi}} \exp\left[\frac{-(\ln D - \ln D_g)^2}{2\ln^2\sigma_g}\right]$$

where D is the diameter (μm), N is a multiplier, σ_g is the geometric standard deviation, and D_g is the geometric mean diameter (μm). The model development was constrained so that (1) it should have a shape similar to the measured average area distributions, (2) the model mass concentration fell near the middle of the mass range it was describing, and (3) the shape of the aerosol model should be consistent at different concentrations (i.e., gradual changes in the distribution as the concentration changes).

Two examples of this manual curve fitting process are given in Figures 6a and 6b, which show the aerosol area size distribution averages for mass range 5.8-11.6 μg/m^3 (Figure 6a) and 0.36-0.72 μg/m^3 (Figure 6b). The resulting model size distributions for that mass range as well as the next smaller range are shown also. Although there is variability in the size distribution at a particular mass range, the general features of the average aerosol distributions are captured in the aerosol model, and the model shape is also preserved for different concentrations. Figures 7a and 7b show all concentrations of the final dry sulfate aerosol model (relative humidity (RH) 0%) plotted as area distributions. As described above, the aerosols tend to gradually shift to larger sizes as the aerosol mass increases. The lognormal parameters for this family of curves are given in Table 1 as number distributions (dN/dlogD) and can be converted to the curves shown in Figure 7 (dA/dlogD) by multiplying the number distribution by the area for each diameter.

Figure 8 compares this accumulation mode aerosol model with other aerosol models developed by *Shettle and Fenn* [1979], *Garthman* [1982], *World Climate Programme* [1983] (WCP-55), and *Shaw* [1979]. All distributions are at 0% relative humidity. Two distributions are shown for our model in order to illustrate the gradual change of the distribution shape with changes in concentration. These are labeled PC3 and PC7 corresponding to cases 4 and 7 in Table 1. It can be seen that our model is narrower than other

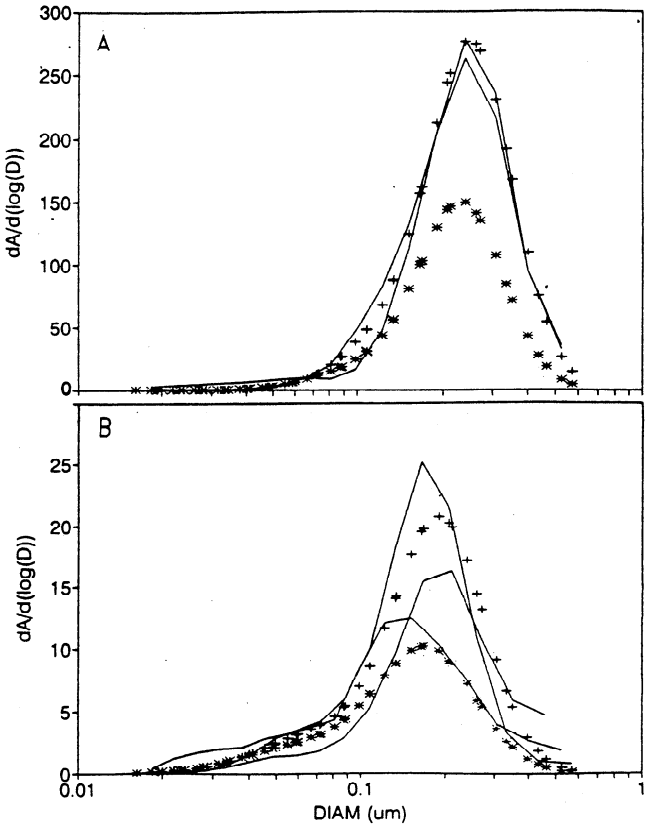

Figure 6. Average measured distributions from the various experiments (solid lines) and two curves illustrating the aerosol model developed here (symbols). Figures 6a and 6b correspond to two different mass categories near the top and bottom of the mass concentration ranges.

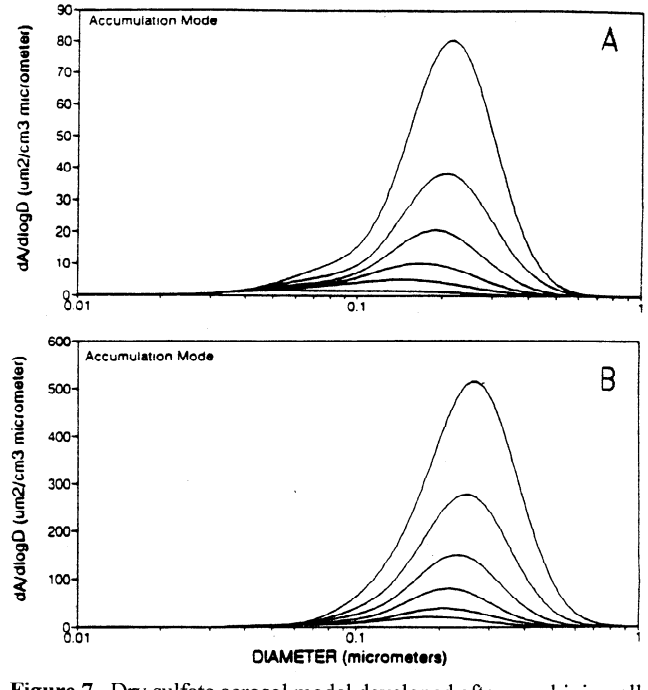

Figure 7. Dry sulfate aerosol model developed after combining all the various experiments. The lognormal parameters for these area distribution curves are given in Table 1 as number distributions. Figure 7a shows distributions 1-6, and Figure 7b shows distributions 4-9.

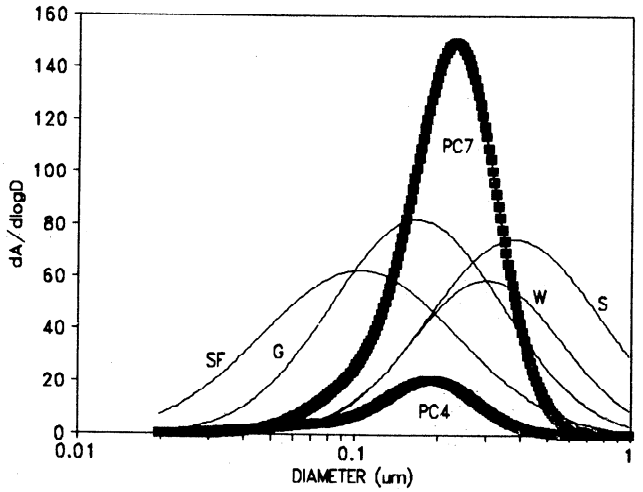

Figure 8. Comparison of various aerosol models for the dry (relative humidity 0%) accumulation mode. Included are *Shettle and Finn* [1979] (SF), *Garthman* [1982] (G), *World Climate Programme* [1983] (W), *Shaw* [1979] (S), and the model developed here, PC4 (curve 4) and PC7 (curve 7).

models for the larger concentrations and has a longer tail at the smaller sizes than at the larger sizes. Our model also tends to fall in the middle range of the other aerosol models, having closest agreement with the WCP-55 and Garthman aerosol models. The substantial variability seen in the different aerosol models suggests further studies are needed until better agreement is obtained from differing sources.

As discussed above, volatility can be used to infer aerosol composition [*Clarke*, 1991]. Figure 9 shows the aerosol volatility of one of the average distributions shown in Figure 4d from the polluted ASTEX measurements. Roughly one fifth of the aerosol area has been removed at 150° C, suggesting the sulfate aerosol is composed of a mixture of H_2SO_4 and $(NH_4)HSO_4$ with a molar ratio $(NH^+_4/SO^=_4)$ near 0.8. The aerosol encountered during the ASTEX experiment ranged from molar ratios below 0.2 to 1.0 with values slightly less than 1.0 occurring most frequently [*A. D. Clarke et al.*, Atmospheric nuclei and related aerosol fields over the Atlantic: Clean subsiding air and continental pollution during ASTEX, submitted to *Journal of Geophysical Research*, 1996; hereinafter referred to as submitted paper, 1996). Over the remote Pacific, molar ratios often range over the same values from 0.2 to 1 [*Clarke and Porter*, 1993; *Porter*, 1988; *Clarke et al.*, 1987].

When aerosols are heated to 300° C, the remaining accumulation mode aerosols are likely to be either sea salt or soot. Aerosol volatility measurements in clean marine regions show that the sea-salt aerosol surface area concentrations are often quite small for diameters below 0.2 μm for wind speeds up to 15 m/s [*Porter*, 1988]. Therefore the peak remaining at 300° C seen in Figure 9 is likely to be anthropogenic soot aerosol as suggested by aerosol light absorption measurements (A. D. Clarke et al., submitted paper 1996).

4. Sea-Salt Coarse Mode Size Distribution

In order to develop an aerosol model for the coarse mode, OPC measurements from the SAGA 2 and SAGA 3 experiments were used. These measurements took place in remote clean marine environments, where contamination by soot or dust was minimal. Similar to the sulfate aerosol model, each measured sea-salt distribution was first grouped by dry aerosol volume. For the coarse mode the aerosols were first heated to 300° C, which volatilized the sulfate accumulation mode. The remaining aerosols were refractory and were composed of either sea salt, dust, or soot. In order to detect the presence of either dust or soot, filter measurements were collected and analyzed for light absorption [*Clarke*, 1989]. Based on the filter light absorption and radon measurements (SAGA 2 and

Table 1. Lognormal Parameters for the Accumulation Mode Aerosol Number Distributions (dN/dlogD)

CASE	HOUR	VOLUME, $\mu m^3/cm^3$	NUMBER, cm^{-3}	CURVE 1 GMD	CURVE 1 STD σ	CURVE 1 MULTIPLIER	CURVE 2 GMD	CURVE 2 STD σ	CURVE 2 MULTI-PLIER
1	0	0.0250	145.3	0.12	1.6	3.4	0.0423	1.65	11.4
2	3	0.075	188.2	0.12	1.6	13.1	0.043	1.65	11.9
3	11	0.150	222.0	0.146	1.5	20.1	0.05	1.65	16
4	81	0.305	267.5	0.167	1.45	33.4	0.0575	1.65	20.4
5	40	0.597	353	0.183	1.44	55.6	0.065	1.65	28
6	18	1.20	515.3	0.195	1.4	100	0.081	1.65	46
7	7	2.40	721.5	0.21	1.4	171	0.1	1.58	72
8	20	4.82	1077	0.227	1.4	289	0.119	1.53	123
9	20	9.60	1766	0.243	1.4	497	0.1310	1.49	230

These distributions are shown as area distributions in Figure 7. The final distribution is the sum of two lognormal curves (see equation). The geometric mean diameter (GMD) (μm), standard deviation (STD), and curve multiplier are given for both curves 1 and 2. Also shown are the integrated volume and integrated number for the total distribution. The first column shows case number and the approximate number of measurement hours which went into each average.

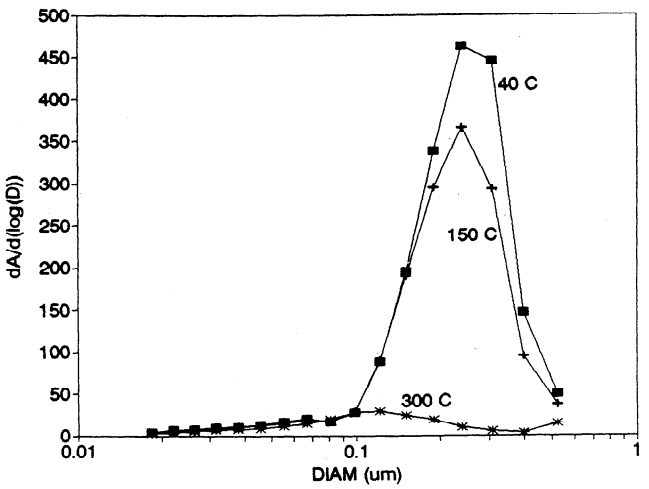

Figure 9. Example of aerosol volatility at 150° and 300° C during the ASTEX experiment. Aerosols remaining after 300 C are inferred to be composed mainly of anthropogenic soot.

SAGA 3 R/V ship report), only the size distributions collected during the cleanest time periods (low radon or light absorption) were used for this study, so that the refractory coarse mode consisted of only sea salt.

As discussed earlier, in order to determine the dry diameter of the accumulation mode, each diameter of the measured distribution had to be shifted to smaller sizes based on the measured instrument relative humidity and Figure 3. This process was not necessary for sea-salt aerosols because they were heated to 300° C and remain dry in the system. This was due to the hysteresis effect of NaCl, which dries out at 40% but does not pick up water until approximately 70% relative humidity [*Tang et al.*, 1977; *Tang and Munkelwitz*, 1977; *Tang*, 1980]. For all cases, the measured relative humidity following the heater in the aerosol sampling system was less than 30% due to both 50% dilution with dry air and system heating of the air stream. Therefore the measured sea-salt aerosols were dry, and no correction for water uptake was applied.

In taking aerosol measurements for the coarse mode, care must be taken to correct for aerosol transmission losses which occur in the sampling system. Details of our approach are given in the work by *Porter et al.* [1992]. In that study the corrected coarse mode aerosol was compared with an external forward scattering spectrometer probe, and good agreement was found under dry conditions. For marine boundary layer cases with high relative humidities, comparisons were not in good agreement, suggesting that unmodeled coarse mode aerosol loss was occurring in the sampling inlet. In order to test the validity of our transmission loss correction, the OPC aerosol distributions were plotted alongside the aerosol measurements performed by *Woodcock* [1953]. Woodcock collected large sea-salt aerosols with a glass slide exposed to ambient air from flying aircraft (~500 to 800 m height), and his measurements should not suffer from any transmission losses. In order to carry out this comparison, OPC aerosol averages were chosen so that they had equal concentrations at the smaller sizes of the Woodcock aerosol distribution where the two distributions overlapped (~0.8-1 μm diameter). While it is true that our measurements are surface measurements (~20 m height), we believe the aerosols below 1 μm are well mixed in the marine boundary layer, so that the two distributions should have similar concentrations below 1 μm diameter. Figure 10 is an example of this type of comparison for one case with very similar concentrations in the overlap region. It suggests significant unmodeled OPC losses are occurring above 2 μm diameter. Other OPC averages had similar results. Therefore, in order to develop a sea-salt model the OPC size distributions were used for the lower portion of the distribution, and the *Woodcock* [1953] aerosol model for the larger diameters. Next a double lognormal curve was used to fit the two data sets. In this process, OPC size distributions were chosen which had similar concentrations with the Woodcock distribution in the region of overlap. Figure 10 shows the final model curve for this case. Figure 11 shows the resulting area distributions (dA/dlogD) for all the sea-salt cases. The lognormal parameters for these area distributions are given in Table 2 as a number distribution (dN/dlogD). The number distributions described in Table 2 can be converted to the area distributions shown in Figure 11 by multiplying by the number at each size by the area of each diameter. The wind speed for each distribution based on Woodcock's measurements is also given in the table. In developing these model cases, some interpolation was required because Woodcock only measured aerosol distributions for Beaufort wind forces of 1, 3, 4, 5, 7 and 12. The resulting aerosol model for the coarse mode is similar to the accumulation mode model, in that as the concentration increases, the peak diameters shift to larger sizes.

Figure 12 compares the sea-salt model with other models developed by *Shettle and Fenn* [1979], *Garthman* [1982] and the *World Climate Programme* [1983] (WCP-55). All distributions are for 0% relative humidity. Two distributions are shown for our model to illustrate the variability in the distribution as the wind speed changes. The *Garthman* [1982] model describes the aerosol model at 80% relative humidity. For Figure 12, it was shifted down by a factor of 1/1.6 to obtain a dry distribution, which is a value close to the growth factors they use. *D'*Almeida et al. [1991] suggest the mixing ratios of the three lognormal components of the WCP-55 are in the model range 0.512-0.667, 0.0042-0.03, and 0.001 for the smallest to largest distributions. In Figure 12 the d'Almeida et al. largest values were used (0.512 and 0.0042) for the distribution (labeled W). Overall, it can be seen that our model tends to fall in the middle of the group. As the wind increases up to

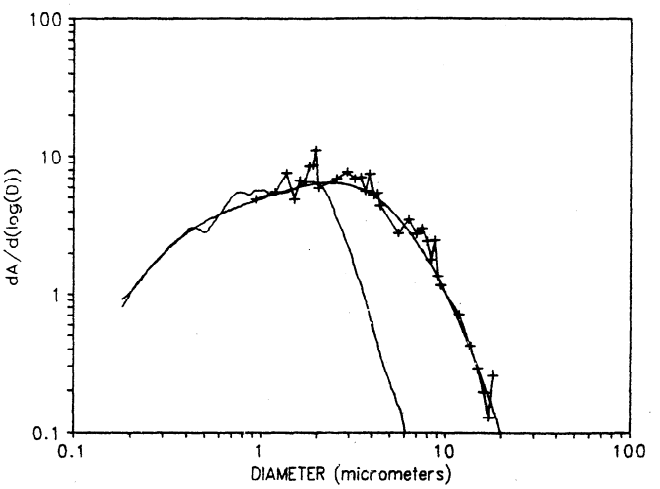

Figure 10. Comparison of the salt aerosol size distribution taken from the optical counter and the *Woodcock* [1953] glass slide impactors. The Woodcock measurements range from 0.9 to 20 μm diameter, while the OPC range from 0.17 to 7.5 μm diameter. The OPC is seriously undercounting above 2 μm diameter. Also shown is the double lognormal curve to fit both distributions and is one of the salt model curves (see equation and Table 2).

Table 2. Log Normal Parameters for Sea Salt Aerosol Number Size Distributions (dN/dlogD).

WIND, m/s	VOLUME, $\mu m^3/cm^3$	NUMBER, cm^{-3}	CURVE 1 GMD	CURVE 1 STD σ	CURVE 1 MULTI-PLIER	CURVE 2 GMD	CURVE 2 STD σ	CURVE 2 MULTI-PLIER
0.4 1.5	0.307	4.143	1.366	1.7	0.2911	0.275	2.00	2.01
1.6 3.3	0.654	5.011	1.407	1.85	0.5277	0.3	2.05	2.57
3.4 5.4	1.50	6.003	1.41	2	1.104	0.308	2.1	3
5.5 7.9	2.74	7.325	1.5	2.1	1.55	0.338	2.23	3.8
8.0 10.7	5.47	8.98	1.51	2.3	2.39	0.349	2.30	4.55
10.8 13.8	8.32	9.9	1.773	2.30	2.53	0.397	2.45	6.07
13.9 17.1	11.8	11.52	2.05	2.30	2.607	0.442	2.55	7.06
17.2 20.7	25.1	13.4	2.807	2.4	2.617	0.4935	2.7	8.9
20.8 24.4	58.6	15.46	3.38	2.55	3.743	0.5	2.8	10
24.5 28.4	129	17.89	4.1	2.64	5.319	0.517	2.88	11.6
28.5 33.5	270	20.77	4.72	2.74	7.96	0.544	2.95	13.7
>33.5	556	25	5.57	2.85	11.4	0.6	3.00	17.8

These distributions are shown as area distributions in Figure 11. The final distribution is the sum of two lognormal curves (see equation). The geometric mean diameter (GMD) (μm), standard deviation (STD), and curve multiplier are given for both curves 1 and 2. Also shown are the integrated volume and integrated number for the total distribution. The first column shows the wind speed based on [*Woodcock*, 1953].

hurricane force, our model shifts to even larger sizes than the WCP-55 model. Above ~1 μm diameter, our model is based on the Woodcock slide measurements and below 1μm, on our thermally resolved OPC measurements.

5. Dust Coarse Mode Size Distribution

During the CPACE aircraft experiment and the MABIE experiment at Mauna Loa (Figure 1) Asian dust was encountered on numerous occasions which provided the opportunity to study the dust properties. In order to develop an aerosol model for this aged Asian dust, the aerosol measurements taken during the MABIE experiment were sorted by dry mass in the same manner as the sea-salt and sulfate distributions in the previous sections. Transmission losses were applied to the distribution prior to processing [*Clarke and Porter*, 1991]. Because the dust aerosols are mostly dry in the atmosphere and can bounce off the sampling wall, it is expected that the error in our modeled transmission will be much less than the wet sea-salt aerosol conditions studied in our aircraft system [*Porter et al.*, 1992]. In order to distinguish between mountain upslope (polluted) and mountain downslope (clean free troposphere) conditions, condensation nuclei concentrations were employed, to determine clean conditions and only these clean downslope cases were used.

The resulting dust aerosol averages from the MABIE experiment are shown in Figure 13, and the lognormal parameters for the number distribution (dN/dlogD) are given in Table 3. From Figure 13 it can be seen that there is a slight shift to larger diameters as the aerosol concentration increases. The lack of large aerosols (above 10 μm diameter) is evident. Similar results reported by *Schutz* [1980] and *Prospero et al.* [1981] suggest that the largest particles fall out with distance away from the source region. Our measurements were some 7000 miles (~11,000 km) downwind from the source. A comparison of our model with the aged dust models of *Shaw* [1979] and *Schutz* [1980] is shown in Figure 14. The fact that our distribution occurs at larger sizes even though the travel distance was further suggests the transport occurred more rapidly,

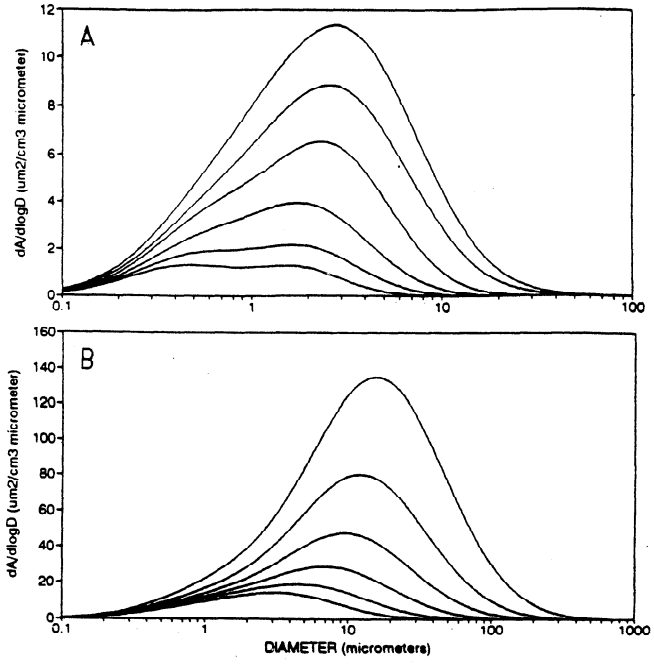

Figure 11. Model dry salt aerosol distributions (shown as area) developed from the combination of OPC and Woodcock size distributions. The curves in Figure 11a correspond to wind speeds of 0.4 to 10.7 m/s, while Figure 11b corresponds to wind speeds from 10.8 to 33.5 m/s. The parameters for these area distributions are given in Table 2 as number distributions.

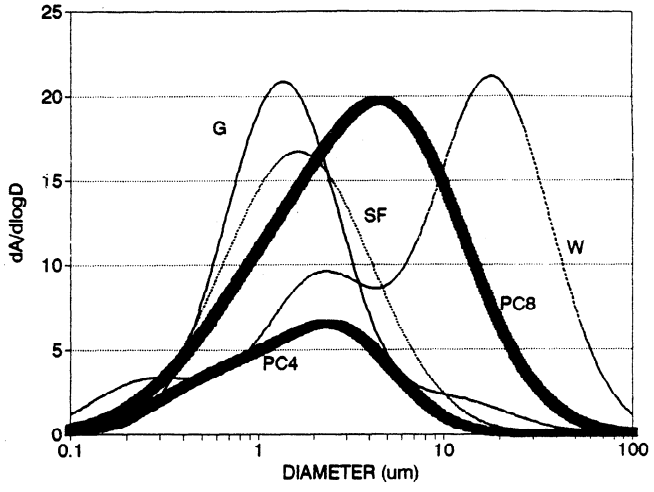

Figure 12. Comparison of various salt aerosol distribution models. Included are *Shettle and Finn* [1979] (SF), *Garthman* [1982] (G), *World Climate Programme* [1983] (W), with the mixing ratios suggested by *d'Almeida et al.* [1991] and the model developed here, PC4 (curve 4) and PC8 (curve 8).

which is consistent with the strong upper troposphere jet stream over the northwest Pacific.

6. Discussion

The aerosol models described here were based on measurements made in various portions of the atmosphere. The sulfate aerosol came from a combination of ship (~20-m height) and aircraft measurements in the boundary layer and lower free troposphere. The resulting aerosol model is therefore intended to represent the aerosol in these regions. The sea-salt measurements below 1 μm diameter were based on our ship measurements (~20-m altitude) and on Woodcock's aircraft measurements for sizes above ~1 μm (~500 to 800-m height). The smaller range of the sea-salt distribution (below 1 μm) is not likely to have strong vertical gradients, so we believe combining the two types of measurements is reasonable. For the larger sizes, sea salt concentrations typically exhibit a strong gradient in the lowest 30 m and smaller gradients above 30 m up to the inversion [*Blanchard et al.*, 1984; *Daniels*, 1989]. Therefore the combined sea salt model is applicable for the marine boundary layer down to 30 m, at which point the largest sizes may not be adequately modeled here. The dust measurements were taken

Table 3. Lognormal Parameters for the Dust Aerosol Number Size Distribution Models

CASE	HOUR	VOLUME, $\mu m^3/cm^3$	NUMBER, cm^{-3}	CURVE 1 GMD	CURVE 1 STD σ	CURVE 1 MULTI-PLIER	CURVE 2 GMD σ	CURVE 2 STD σ	CURVE 2 MULTI-PLIER
2	27	0.0226	0.0435	2.580	1.45	0.006172	0.6967	1.95	0.0484
3	17	0.0772	0.0874	2.315	1.55	0.02425	0.7896	1.90	0.1008
4	23	0.189	0.1484	2.384	1.55	0.03053	0.8084	2.27	0.1906
5	56	0.376	0.247	2.860	1.55	0.05830	0.8680	2.27	0.3364
6	8	0.764	0.409	3.065	1.55	0.09235	0.8858	2.25	0.6209
7	2	1.33	0.681	3.133	1.55	0.1767	0.9518	2.20	1.014
8	2	2.81	1.15	3.201	1.55	0.4233	0.9806	2.20	1.910
9	1	5.72	1.74	3.729	1.60	0.6622	1.038	2.20	2.896

These distributions are shown as area distributions in Figure 13. The final distribution is the sum of two lognormal curves (see equation). The geometric mean diameter (GMD) (μm), standard deviation (STD), and curve multiplier are given for both curves 1 and 2. Also shown are the integrated volume and integrated number for the total distribution. The first column shows case number and the approximate number of measurement hours which went into each average.

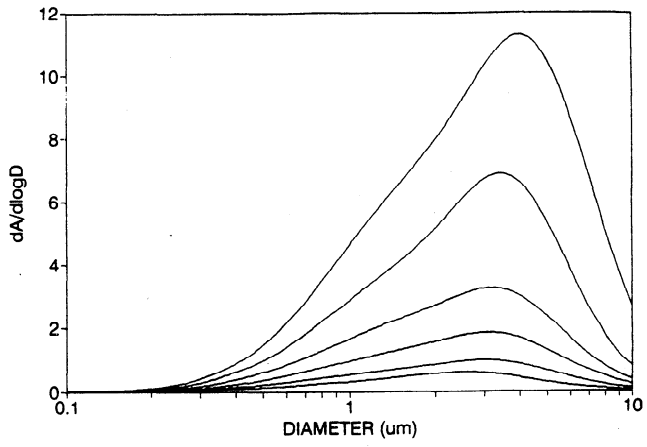

Figure 13. The model dust (cases 4-9) aerosol area size distributions developed from measurements taken at Mauna Loa Observatory, Hawaii. The parameters for these area distributions are given in Table 3 as number distributions.

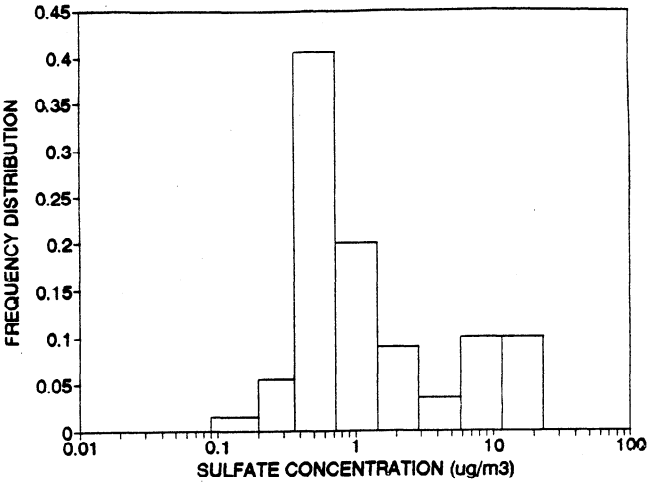

Figure 15. Normalized frequency distribution of sulfate aerosol concentrations measured on the SAGA 3, *Kaiyoumaru* and ASTEX experiments. Two main modes appear which correspond to remote aerosol concentrations and anthropogenically affected periods.

in Hawaii above the trade wind inversion (the free troposphere) and represent aged central Pacific dust cases.

As shown in Figures 7, 11 and 13, the aerosol peak diameter shifts to larger sizes as the aerosol mass increases. This relationship creates the possibility to estimate the aerosol size distribution based on aerosol mass measurements (i.e., filter measurements). The uncertainty in these estimates depends on how representative our measurements are on a global scale and the variability in our data set. The variability of the accumulation mode peak diameter was found to have an average one standard deviation of 0.027. The accumulation mode diameter shift, from one size distribution to the next, was on average 0.023 μm. Therefore the distribution for a particular mass range may vary up and down to the adjacent model size distributions as a one standard deviation.

The second type of error, which is impossible to avoid, is the fact that our measurements are finite (i.e., they were made over limited space and time), resulting in some amount of bias. Although this bias will be present in any data set, we believe it is minimized here by the spatial diversity of our measurements, which took place over broad expanses of the Pacific and Atlantic Oceans. The ASTEX and CPACE aircraft measurements occurred over approximately a 30-day period with measurements being made on half of these days in a range of meteorological conditions and altitudes. The ship measurements covered broad ranges of the Pacific Ocean and ranged from midlatitude through tropical regimes.

One way to test how representative the aerosol is on a global scale is to compare it with other aerosol mass measurements to make sure that the most common aerosol concentrations occurring in our data appear in other data sets as well. Figure 15 shows the normalized mass frequency distribution for the DMA measurements. Two main modes are evident. One mode with an effective mass concentration of 0.55 $\mu g/m^3$ is representative of remote marine regions, and the second mode (~12 $\mu g/m^3$) is due to anthropogenic pollution recently advected over the ocean. *Pruppacher and Klett* [1980] report average urban sulfate concentrations of 10.1 $\mu g/m^3$ based on the measurements of *Ludwig et al.* [1971]. *D'Almeida et al.*[1991] compiled the results of *Saltzman et al.* [1985], *Savoie et al.* [1987], and *Clarke et al.*, [1987] for clean marine environments. The average non-sea-salt sulfate concentration is 0.62 $\mu g/m^3$. These literature values are reasonably consistent with the most common values appearing in Figure 15 and suggest our measurements reflect the major aerosol properties needed to model marine aerosol on global scales. On the other hand, the large differences in the various aerosol models seen in Figures 8, 12, and 14 suggest further measuring and modeling efforts will be needed.

We found the peak of both the accumulation and coarse modes shifts to larger sizes as the aerosol mode mass increases. For sea salt and dust this is easy to understand, as stronger winds which lift more aerosol can also support large aerosol, causing a shift to larger sizes and viceversa for light winds. The shift in the sulfate accumulation mode is more complex, and several possibilities might account for this behavior. First is the fact that the aerosol removal processes (cloud precipitation for the activated aerosol) tends to remove the largest aerosol first. Therefore any time the aerosol concentration is lowered, the effective aerosol diameter is also shifted to lower diameters. The aerosol coagulation rate should also increase as the aerosol surface area increases [*Pruppacher and Klett*, 1980]. This process is evident in the stratosphere, where

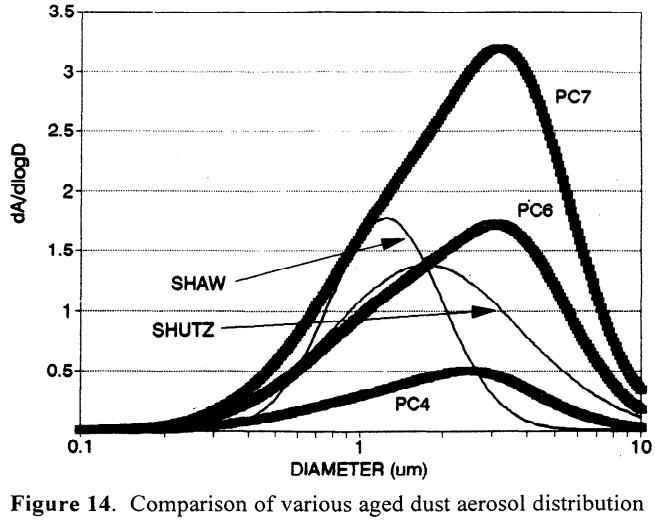

Figure 14. Comparison of various aged dust aerosol distribution models. Included are *Schutz* [1980] and *Shaw* [1979] and the model developed here (PC4 (curve 4), PC6 (curve 6), and PC7 (curve 7)).

aerosol lifetimes are long and the aerosols shift to very large sizes [*Zhao et al.*, 1995]. Cloud processing will also shift the activated aerosol to larger sizes by gas to particle conversion in cloud drops [*Hoppel et al.*, 1994]. Counteracting this simple conceptual model is the fact that mixing between different air masses will dilute polluted air, resulting in lower mass concentrations with size distributions which are still representative of the previous concentration. Despite this broadening effect, the trend to larger sizes with increasing mass is evident in our measurements.

Acknowledgments. The present study was funded by a NASA climate change student fellowship, NSF grant ATM90-01434, ONR grant 14-92-J-1388, and NASA grant NAGW3766. SOEST contribution 4176, HIGP contribution 926.

References

Blanchard, D.C., A.H. Woodcock, and R.J. Cypriano, The vertical distribution of sea salt in the marine atmosphere near Hawaii, *Tellus, Sec. B, 36*, 118-125, 1984.

Clarke A.D., Aerosol light absorption by soot in the remote environments, *Aerosol Sci. Technol., 10*, 161-171, 1989.

Clarke, A.D., A thermo-optic technique for in situ analysis of size resolved aerosol physicochemistry, *Atmos. Environ.*, part A, 25, 635-644, 1991.

Clarke, A.D., and J.N. Porter, Aerosol size distributions, composition, and CO_2 backscatter, *J. Geophys. Res., 96*, 5237-5247, 1991.

Clarke, A.D., and J.N Porter, Pacific marine aerosol, 2, Equatorial gradients in chlorophyll, ammonium, and excess sulfate during SAGA 3, *J. Geophys.Res., 98*, 16,997-17,010, 1993.

Clarke, A.D., N.C. Ahlquist, and D.S. Covert, The Pacific marine aerosol: Evidence for acid sulfates, *J. Geophys. Res., 92*, 4179-4190, 1987.

Clarke, A.D, J.N. Porter, F.P.J. Valero, and P. Pilewskie, Vertical profiles, aerosol microphysics, and optical closure during the Atlantic Stratocumulus Transition Experiment: Measured and modeled column optical properties, *J. Geophys. Res., 101*, 4443-4453, 1996.

Covert, D.S., V.N. Kapustin, P.K. Quinn, and T.S. Bates, New particle formation in the marine boundary layer. *J. Geophys. Res., 97*, 20,581-20,589, 1992.

d'Almeida, G.A., P. Koepke, E.P. Shettle, *Atmospheric Aerosols: Global Climatology and Radiative Characteristics*, A. Deepak, Hampton, Va., 1991.

Daniels, A., Measurements of atmospheric sea salt concentrations in Hawaii using a tala kite. *Tellus, Sec. B, 41*, 196-206, 1989.

Garthman, S.G., A time dependent oceanic aerosol model, *Tech. Rep. 8536*, 35 pp. Nav. Res. Lab., Washington, D.C., 1982.

Garthman, S.G., *Navy Hygroscopic Aerosol Model: Hygroscopic Aerosol*, A. Deepak, Hampton, Va., 1984.

Hoppel, W.A., Measurements of the size distribution and CCN supersaturation spectrum of submicron aerosols over the ocean, *J. Atmos. Sci., 9*, 41-54, 1979.

Hoppel, W.A., G.M. Frick, and J.W. Fitzgerald, Marine boundary layer measurements of new particle formation and the effects nonprecipiting clouds have on aerosol size distribution, *J. Geophys. Res., 99*, 14,443-14,459, 1994.

Ludwig, J.H., G.B. Morgan, and T.B. McMullen, Man's impact on Climate , edited by Matthews et al., p. 321, MIT Press, Cambridge, Mass., 1971.

Porter, J.N., Marine aerosol: Their measurement and influence on cloud base properties, Masters thesis, Univ. of Hawaii, Honolulu, 1988.

Porter, J.N., A.D. Clarke, G. Ferry, and R.F. Pueschel, Aircraft studies of size dependent aerosol sampling through inlets, *J. Geophys. Res., 87*, 3815-3824, 1992.

Prospero, J.M., R.A. Glaccum, and R.T. Nees, Atmospheric transport of soil dust from Africa to South America, *Nature, 289*, 570-572, 1981.

Pruppacher, H.R., and J.D. Klett, *Microphysics of Clouds and Precipitation*, D. Reidel, Nowell, Mass., 1980.

Reist, P.C., *Introduction to Aerosol Science*, Macmillan, New York, 1984.

Remer. L.A., Y.J. Kaufman, and B.N. Holben, The size distribution of ambient aerosol particles, in *Biomass Burning and Global Change*, edited by J.S. Levine, MIT Press, Cambridge, Mass., 1996.

Saltzman, E.S., D.L. Savoie, J.M. Prospero, and R.G. Zika, Atmospheric methansulfonic acid and non-sea-salt sulfate at Fanning and American Samoa, *Geophys. Res. Lett., 12*, 437-440, 1985.

Savoie, D.L., J.M. Prospero, and R.T. Nees, Washout ration of nitrate, non-sea-salt-sulfate, and sea salt on Virginia Key, Florida, and on America Samoa, *Atmos. Environ., 21*, 103-112, 1987.

Schutz, L., Long-range transport of desert dust with special emphasis on the Sahara, *Ann. N.Y. Acad. Sci., 338*, 515-532, 1980.

Shaw, G.E., Consideration on the origin and properties of the Antartic acrosol. *Rev. Geophys., 17*, 1983-1998, 1979.

Shettle, E.P., and R.W. Fenn, Models for the aerosols of the lower atmosphere and the effects of humidity variations on their optical properties, *Rep. AFGL TR-79-0214, AD-A085951*, 94 pp., Air Force Geophys. Lab., Bedford, Mass., 1979. (Available as *AD-A197945* from Natl. Tech. Inf. Serv., Springfield, Va.)

Tang, I.N., Deliquescence properties and particle size change of hygroscopic aerosols in *Generation of Aerosol*, 153 pp., Butterworth-Heinemann, New Mass., 1980.

Tang, I.N., and H.R. Munkelwitz, Aerosol growth studies, III, Ammonium bisulfate aerosols in a moist atmosphere, *J. Aerosol Sci.*, 8, 321-330, 1977.

Tang, I.N., H.R. Munkelwitz, and J.G. Davis, Aerosol growth studies, II, Preparation and growth measurements of monodisperse salt aerosols, *J. Aerosol Sci.*, 8, 149-159, 1977.

Whitby, K.T., The physical characteristics of sulfur aerosols, *Atmos. Environ., 12*, 135-159, 1978.

Woodcock, A.H., Salt nuclei in marine air as a function of altitude and wind force, *J. Meteorol., 10*, 362-371, 1953.

World Climate Programme, Report of the expert meeting on aerosols and their climatic effects, *WCP-55*, edited by A. Deepak and H. E. Gerber, World Meteorol. Organ., Geneva, 1983.

Zhao, J., R.P. Turco, and O.B. Toon, A model simulation of pinatubo volcanic aerosols in the stratosphere, *J. Geophys. Res., 100*, 7315-7328, 1995.

A.D. Clarke and J. Porter, School of Ocean and Earth Science and Technology, University of Hawaii, 2525 Correa Road, Honolulu HI 96822.

(Received December 29, 1993; revised October 28, 1996; accepted October 28, 1996.)